JGR Atmospheres

RESEARCH ARTICLE
10.1029/2021JD035987

Global Daily Actual and Snow-Free Blue-Sky Land Surface Albedo Climatology From 20-Year MODIS Products

Aolin Jia[1], Dongdong Wang[1], Shunlin Liang[1], Jingjing Peng[2], and Yunyue Yu[2]

[1]Department of Geographical Sciences, University of Maryland, College Park, MD, USA, [2]NOAA/NESDIS Center for Satellite Application and Research, College Park, MD, USA

Key Points:

- A global 500 m daily blue-sky land surface albedo climatology data set in actual and snow-free surface conditions was produced from Moderate Resolution Imaging Spectroradiometer
- Site validation and data comparison reveal its reliability and robustness in model assessment, data assimilation, and satellite retrievals
- Simulated albedo data by state-of-art reanalysis and Coupled Model Intercomparison Projects Phase 6 models still have a clear bias in polar regions and the Tibetan Plateau

Correspondence to:
S. Liang,
sliang@umd.edu

Citation:
Jia, A., Wang, D., Liang, S., Peng, J., & Yu, Y. (2022). Global daily actual and snow-free blue-sky land surface albedo climatology from 20-year MODIS products. *Journal of Geophysical Research: Atmospheres*, *127*, e2021JD035987. https://doi.org/10.1029/2021JD035987

Received 5 OCT 2021
Accepted 28 MAR 2022

Author Contributions:
Conceptualization: Aolin Jia, Dongdong Wang, Shunlin Liang, Jingjing Peng, Yunyue Yu
Data curation: Aolin Jia
Funding acquisition: Dongdong Wang, Shunlin Liang
Investigation: Aolin Jia, Dongdong Wang, Jingjing Peng
Methodology: Aolin Jia, Dongdong Wang, Shunlin Liang
Project Administration: Dongdong Wang, Shunlin Liang, Yunyue Yu
Software: Aolin Jia
Supervision: Shunlin Liang
Validation: Aolin Jia, Jingjing Peng
Writing – original draft: Aolin Jia
Writing – review & editing: Aolin Jia, Dongdong Wang, Shunlin Liang, Jingjing Peng, Yunyue Yu

Abstract Land surface albedo plays a critical role in climate, hydrological and biogeochemical modeling, and weather forecasting. It is often assigned in models and satellite retrievals by albedo climatology look-up tables using land cover type and other variables; however, there are considerable differences in albedo simulations among models, which partially result from uncertainty in obsolete albedo climatology. Therefore, this study introduces a new global 500 m daily blue-sky land surface albedo climatology data set under both actual and snow-free surface conditions utilizing 20-year Moderate Resolution Imaging Spectroradiometer products from Google Earth Engine. *In situ* measurements from 38 long-term-maintained sites were utilized to validate the accuracies of different albedo climatology datasets. The root-mean-square error, bias, and correlation coefficient of the new climatology are 0.031, −0.003, and 0.96, respectively, which are more accurate than the Global Land Surface Satellite, GlobAlbedo, and 16 model datasets. Data intercomparison suggests that ERA5 exhibits better performance than Modern-Era Retrospective Analysis for Research and Applications Version 2 (MERRA2) and 14 Coupled Model Intercomparison Projects Phase 6 models. However, it contains positive biases in the snow-free season, while MERRA2 underestimates the snow albedo. Global albedo variation associated with basic surface plant functional types was also characterized, and snow impact was considered separately. Temporal variability analysis indicates that traditional climatology datasets with coarser temporal resolutions (≥8 days) cannot capture albedo variation over areas with distinct snow seasons, especially in central Eurasia and boreal regions. These results confirm the high reliability and robustness of the new albedo climatology in model assessment, data assimilation, and satellite product retrievals.

Plain Language Summary Surface albedo represents the Earth's surface ability to reflect solar energy, and thus directly influences atmospheric and water circulations by controlling available energies. As an essential variable estimated in current climate models, surface albedo is assigned by searching look-up tables based on the land cover and soil types. However, there are large differences in simulated albedo among various models, partially because the albedo climatology in these tables was generated in the 1980s and needs to be updated. As global surface albedo has been accurately retrieved from satellite data for decades, we were able to produce a new albedo climatology data set under actual and snow-free conditions with high spatiotemporal resolutions. Ground validation and data comparison indicate that the new data set performs with higher accuracy compared with other datasets. Moreover, assessment by the new climatology data set shows that albedo from advanced climate models and reanalysis datasets has clear uncertainties, especially over high latitudes and the Tibetan Plateau. Temporal variation in global albedo is better characterized at basic vegetation types. The new albedo climatology data set shows great potential for use in model assessment, modeling improvement, and satellite retrieval of other variables.

1. Introduction

Land surface albedo, which is defined as the ratio of the reflected shortwave radiation to the incoming solar radiation, represents the integrated surface hemispheric reflectivity over the solar spectrum (Liang et al., 2010; Lucht et al., 2000). It is a critical geographical parameter that directly controls the surface radiation budget between the surface and atmosphere, significantly affecting the energy budget, and atmospheric and water circulations (Boussetta et al., 2015; Liang et al., 2010). Therefore, it is listed as an Essential Climate Variable (GCOS, 2004) and basic climate forcing used in hydrological, and biogeochemical models, as well as in weather forecasting (Graversen & Wang, 2009; Houldcroft et al., 2009; Van Angelen et al., 2012). In remote sensing retrieval algorithms (Rutan et al., 2009, 2015; Wang et al., 2020) and climate and ecosystem models (Dickinson, 1995; Grey et al., 2009; Wang et al., 2004), the surface albedo is generally assigned by look-up-tables (LUTs) of albedo

climatology (albedo values averaged over decades) based on land cover types and other variables (such as snow cover fraction and leaf area index) (Lawrence et al., 2019). However, the comparison of the surface albedo derived from different models indicates clear differences (Levine & Boos, 2017), especially in high-latitude regions (Thackeray et al., 2019; Zhang et al., 2010), leading to considerable uncertainty of surface energy balance estimations. Besides, current state-of-art Community Land Models still employ the albedo LUTs generated by satellite data decades ago (Asner et al., 1998; Dorman & Sellers, 1989; Lawrence et al., 2020). Thus, the accuracy of the albedo climatology significantly affects the modeling predictions (Burakowski et al., 2018; Gao et al., 2014; Masson et al., 2013). Moreover, most satellite-derived albedo data are only available for clear-sky conditions, whereas the albedo climatology characterizes a general gap-free albedo pattern, providing important information for estimating the surface albedo under cloudy conditions (Liu et al., 2013; Wang et al., 2015; Zhou et al., 2016). As land surface albedo is controlled by the land type, vegetation growth, and snow coverage, it is highly variable, both spatially and temporally. Therefore, precisely mapping the global surface albedo climatology is necessary to better characterize the energy budget of the Earth system.

Satellite remote sensing has been used to monitor the global land surface and record the albedo over the long term (Liang et al., 2013), providing the only possibility for generating global surface albedo climatology. Currently, satellite albedo products have become accessible through a wealth of sensors such as the Moderate Resolution Imaging Spectroradiometer (MODIS; (Liu et al., 2013; Strahler et al., 1999)), Visible Infrared Imaging Radiometer Suite (VIIRS; (Wang et al., 2013, 2016)), Advanced Very High-Resolution Radiometer (AVHRR (Karlsson et al., 2013; Liu et al., 2013)), Spinning Enhanced Visible and Infrared Imager (SEVIRI (Geiger et al., 2008)), and SPOT/VEGETATION (Barnsley et al., 2000). A comprehensive algorithm review was conducted by Qu et al. (2015). However, most albedo products only provide directional- and bi-hemispherical albedo (i.e., black-sky albedo, BSA, and white-sky albedo, WSA) maps. In contrast, blue-sky albedo is the actual albedo and is more practical for analysis. The combination of the MODIS albedo product (Schaaf et al., 2002), which was published over 20 years ago, with the MODIS aerosol product has great potential for the generation of the global surface blue-sky albedo climatology with high spatial and temporal resolutions.

Previous studies have focused on generating satellite-derived albedo climatology databases or LUTs. Carrer et al. (2014) generated global snow-free vegetation and baer soil albedo maps from 10-year MODIS data products. He et al. (2014) compared the spatiotemporal differences of several global albedo climatology data from operational satellite products and quantified the monthly albedo variations of different plant functional types (PFTs). Gao et al. (2014) generated climatological albedo LUT using MODIS albedo products with a global International Geosphere-Biosphere Programme (IGBP) classification map at different spatial scales. They also tested the variability of the albedo for 17 IGBP classes (Gao et al., 2005). However, the above-mentioned albedo climatology databases are limited by coarse spatial ($\geq$0.05°) and temporal (monthly) resolutions, which are insufficient to capture the spatial heterogeneity and temporal dynamics of the albedo, especially in the snow season. In addition, they only consider either snow-covered or snow-free conditions, although the effect of snow on surface albedo varies depending on the vegetation type and must be separately studied. By combining National Land Cover Data (NLCD) with the MODIS albedo, Wickham et al. (2015) created a land cover–albedo database based on 14 years of snow-covered and snow-free MODIS albedo data for 14 of 16 land cover classes in the NLCD; however, the study only included the continental United States. Therefore, a new albedo climatology with high spatiotemporal resolution and global coverage is required.

The contributions of this study are as follows: (a) Global actual (all historical records including the snow albedo) and snow-free daily blue-sky albedo climatology datasets were generated and published, including land cover climatology at 500 m, 0.05°, and 0.5° resolutions; (b) the generated climatology datasets were validated using 38 long-term-operating *in situ* sites in different land cover types; (c) multiple albedo climatology datasets from satellite products, reanalysis, and state-of-art Coupled Model Intercomparison Projects Phase 6 models were first assessed globally and compared; (d) global error patterns of the model datasets were determined by using the new albedo climatology as a reference; (e) the global actual and snow-free albedo variations of different PFTs were analyzed; and (f) temporal variability analysis was conducted with respect to the temporal aggregation of the new climatology data set.

Table 1
Metadata of the Moderate Resolution Imaging Spectroradiometer Products, Reanalysis, and Coupled Model Intercomparison Projects Phase 6 Data Utilized in This Study

Name	Variables	Spatial resolution	Temporal resolution	Reference
MCD43A3	BSA, WSA	500 m	daily	Schaaf and Wang (2015b)
MCD43A2	snow mark, SZA	500 m	daily	Schaaf and Wang (2015a)
MOD08M3	AOD	1° × 1°	monthly	Platnick et al. (2015)
MCD12Q1	LC_Type_5	500 m	yearly	Sulla-Menashe and Friedl (2018)
GLASS	BSA, WSA	1 km	8-day	Liang et al. (2021)
GlobAlbedo	BSA, WSA	1 km	8-day	Muller (2013)
ERA5-Land	surface albedo	0.1° × 0.1°	hourly	Hersbach et al. (2020)
MERRA2	surface albedo	1° × 1°	hourly	Molod et al. (2015)
BCC-CSM2-MR	RSDS, RSUS	1.13° × 1.13°	3-hourly	Wu et al. (2019)
BCC-ESM1	RSDS, RSUS	2.81° × 2.81°	3-hourly	Wu et al. (2020)
CanESM5	RSDS, RSUS	2.81° × 2.81°	3-hourly	Swart et al. (2019)
CESM2	RSDS, RSUS	0.94° × 1.25°	3-hourly	Danabasoglu et al. (2020)
CESM2-FV2	RSDS, RSUS	1.88° × 2.50°	3-hourly	Danabasoglu et al. (2019)
CESM2-WACCM	RSDS, RSUS	0.94° × 1.25°	3-hourly	Danabasoglu et al. (2019)
CESM2-WACCM-FV2	RSDS, RSUS	1.88° × 2.50°	3-hourly	Danabasoglu et al. (2019)
FGOALS-f3-L	RSDS, RSUS	1° × 1.25°	3-hourly	He et al. (2019)
FGOALS-g3	RSDS, RSUS	2.25° × 2°	3-hourly	Li et al. (2020)
KIOST-ESM	RSDS, RSUS	1.96° × 1.88°	3-hourly	Kim et al. (2020)
MIROC6	RSDS, RSUS	1.41° × 1.41°	3-hourly	Tatebe et al. (2019)
MRI-ESM2-0	RSDS, RSUS	1.13° × 1.13°	3-hourly	Yukimoto et al. (2019)
NESM3	RSDS, RSUS	1.88° × 1.88°	3-hourly	Cao et al. (2018)
SAM0-UNICON	RSDS, RSUS	0.94° × 1.25°	3-hourly	Park et al. (2019)

Note. The data ranges from 2001 to 2020.

2. Data and Methodology

2.1. Data

In this study, new blue-sky albedo climatology data were validated by 38 sites of the Surface Radiation (SURFRAD), Baseline Surface Radiation Network (BSRN), and Fluxnet networks. Other albedo climatology data, such as the albedo product from the Global Land Surface Satellite (GLASS) product suite, GlobAlbedo satellite product, European Centre for Medium-Range Weather Forecasts (ECMWF) Reanalysis 5 (ERA5), Modern-Era Retrospective Analysis for Research and Applications Version 2 (MERRA2), and 14 CMIP6 models, were included for comparison. The metadata and references for all gridded data are summarized in Table 1. The sites are mapped in Figure 1.

2.1.1. MODIS Products

Global MODIS 500-m daily shortwave black-sky and white-sky albedo (MCD43A3 C06) data from 2001 to 2020 were used to calculate the blue-sky albedo climatology. The MODIS albedo products utilize a semi-empirical linear kernel-driven model and estimate albedo with a bidirectional reflectance distribution function (BRDF) (Lucht et al., 2000). It has been comprehensively assessed (He et al., 2012; Stroeve et al., 2005; Wang et al., 2012) and extensively used as a benchmark for the evaluation of other albedo datasets (Lawrence & Chase, 2007; Li et al., 2016).

To generate actual and snow-free albedo climatology data, the corresponding snow mark from MCD43A2 C06 was used for the classification of snow or snow-free albedo pixels. The aerosol optical depth (AOD) at 0.55 μm from the MODIS gridded atmosphere global joint product (MOD08 C61) was selected to obtain the diffuse

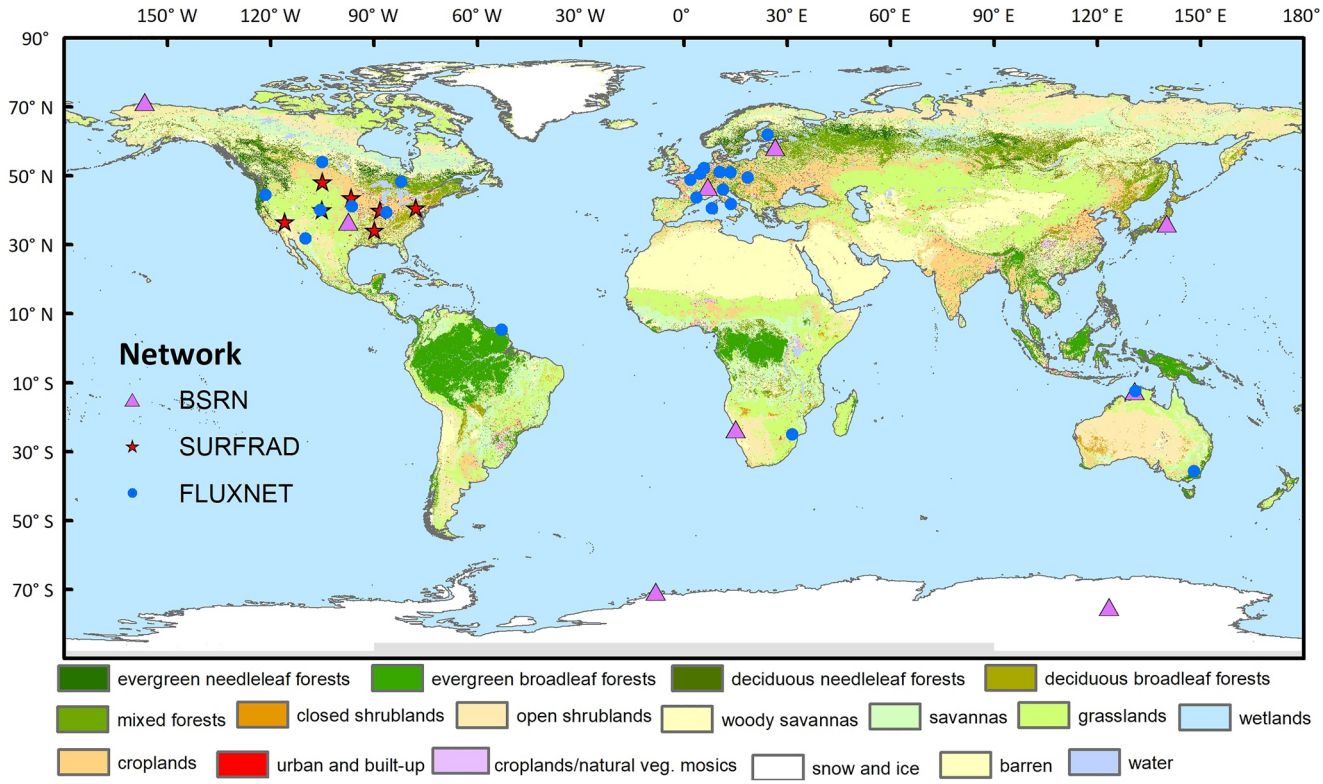

Figure 1. Global distribution of the 38 sites with land cover types.

skylight ratio, which was used to compute the blue-sky albedo (Section 2.2.1). The PFT climatology, classified by the MODIS surface land cover type product (MCD12Q1) from 2001 to 2020, was used to characterize the albedo variation of different PFTs.

To compare the validation accuracy between the new albedo climatology and other satellite products, albedo climatology samples from the GLASS albedo product (Liang et al., 2021; Liu et al., 2013) were also validated in the site assessment section. The GLASS albedo was retrieved from MODIS observations based on two direct albedo estimation algorithms: surface reflectance and top-of-atmosphere (TOA) reflectance algorithms (Qu et al., 2014). Subsequently, a statistics-based temporal filtering method was employed to fuse the two albedo products, whose accuracy was comparable to that of the MODIS albedo product (Liu et al., 2013). Finally, the GLASS blue-sky albedo climatology was generated similar to the MODIS from 2001 to 2019 (the latest year accessible).

The albedo climatology from the GlobAlbedo project was also involved. The 1 km 8-day BSA and WSA from 2000 to 2011 were utilized for this purpose. GlobAlbedo aims to create gap-filled global albedo data by integrating data from the Advanced Along-Track Scanning Radiometer (AATSR), Medium-Resolution Imaging Spectrometer (MERIS), SPOT/VEGETATION, and MODIS (Muller et al., 2012). An optimal estimation method was used for data fusion and the gap-filling approach was based on MODIS surface anisotropy data (Lewis et al., 2012). The blue-sky albedo was calculated and then averaged to obtain climatology samples.

2.1.2. Reanalysis and CMIP6 Datasets

ERA5, which is the new generation of a widely used reanalysis product (Hersbach et al., 2020), was employed for the assessment in this study. ERA5 is the fifth generation of the atmospheric reanalysis of the global climate from 1950 to near real-time. It is based on four-dimensional variational analysis (4DVAR) and features different physical parameterizations. ERA5 uses the Radiative Transfer for Television Infrared Observation Satellite Operational Vertical Sounder (RTTOV)-11 model as the observation operator for radiance data (Lupu & Geer, 2015). The radiation scheme used in ERA5 was described by Morcrette et al. (2008). In the ECMWF Integrated Forecasting System (IFS), a monthly climatological background albedo from MODIS is assimilated, after modification by

the model over water, ice, and snow (Di Napoli et al., 2020; Muñoz-Sabater et al., 2021). Snow data observed by Surface synoptic (SYNOP) network are used in the snow assimilation system. The ERA5-Land hourly surface albedo from 2001 to 2020 was collected. To be comparable with MODIS albedo results, only the local noon blue-sky albedo climatology for each pixel and Day of Year (DOY) were generated (Schaaf et al., 2011).

The National Aeronautics and Space Administration (NASA) MERRA2 was included in the assessment as another advanced reanalysis data set. MERRA was created to provide context for NASA satellite data, with the specific goal of better representing the hydrologic cycle than existing reanalysis data (Hinkelman, 2019). MERRA2 employs 3DVAR and updates the performance of the model in both the atmosphere-only and atmosphere-ocean configurations (Molod et al., 2015). The longwave and shortwave radiative processes were based on Suarez and Chou (1994) and Chou and Suarez (1999), respectively. The temporally interpolated MODIS albedo product was assimilated into the model (Cullather & Bosilovich, 2012; Moody et al., 2005). The hourly surface albedo from 2001 to 2020 was used to generate the local noon blue-sky albedo climatology for each pixel, similar to ERA5 data.

Coordinated efforts have been made to constantly update climate models in CMIP. As the next-generation global climate model (GCM), CMIP6 is featured in the 2021 Intergovernmental Panel on Climate Change (IPCC) sixth assessment report (AR6). Several basic outcomes from CMIP6 have recently been assessed using site measurements and satellite observations, such as the planetary albedo (Jian et al., 2020), snow cover (Zhu et al., 2021), sea ice extent (Shu et al., 2020), water fluxes (Li et al., 2021), cloud fraction (Vignesh et al., 2020), air temperature and precipitation (Cui et al., 2021), and surface upward longwave radiation (Xu et al., 2021). However, as an essential climate driver, land surface albedo from CMIP6 GCMs remains to be explored. Surface albedo showed systematic overestimation in the seasonal cycle simulated by CMIP5 GCMs (Li et al., 2016), and we would like to analyze the bias issue to see if there is any significant improvement. Therefore, surface albedo climatology datasets from published CMIP6 models were used for the assessment in this study. Based on a further comparison with the newly generated climatology, the uncertainty of the modeled surface albedo was quantified. The surface downward shortwave radiation (RSDS) and surface upward shortwave radiation (RSUS) were obtained to calculate the albedo climatology from actual CMIP6 experiments (2001–2014) and extended (2015–2020) using Shared Socioeconomic Pathways (SSP) 2–4.5 scenario experiments. In addition, to reduce the data volume, only the first ensemble member ("r1i1p1f1") was used for each model. Fourteen available models meet the requirements.

2.1.3. In Situ Sites

Albedo accuracy requirement varies from 0.02 to 0.05 (or 5%) for climate-related studies (Li & Garand, 1994; Oleson et al., 2003). Therefore, ground validation is necessary to assess the absolute accuracy of climatological datasets. Here, 38 long-term-operated sites of the SURFRAD (7), BSRN (9), and Fluxnet (22) networks were utilized to quantify the absolute accuracy of the surface albedo climatology datasets at the global scale.

Established in 1993, SURFRAD was designed to support climate research with accurate, continuous, long-term measurements of the surface radiation budget over the United States (Augustine et al., 2000), and has been widely used for the validation of surface radiation fluxes (Jia, Ma, et al., 2021; Li et al., 2013; Wang & Liang, 2009; Zhou et al., 2016). The BSRN is a network (Driemel et al., 2018) of globally distributed sites collecting data for different projects, including the Coordinated Energy and Water Cycle Observations Project (CEOP) and AmeriFlux, and is considered to have the longest duration and good quality owing to the strict maintenance (Wang & Dickinson, 2013). Fluxnet, which monitors the global energy budget, water and carbon cycling, was also employed in this study to ensure site global coverage (Wilson et al., 2002). Fluxnet has previously been used in surface albedo validation (Cescatti et al., 2012). Raw observations were well filtered by quality control marks and thresholds (Roesch et al., 2011). For all three networks, sites with more than 10 years of operation were selected for calculating the surface albedo climatology. Compared with SURFRAD and BSRN, duplicated sites or sites within a close distance (500 m) of Fluxnet were removed. Additionally, ground measurements from different sites were averaged if the sites were located within the same coarse model pixel. The local noon blue-sky albedo was calculated by averaging the observations from 12:00 to 13:00 local time (LT) to remove anomalous values. Site distribution and corresponding land cover types are shown in Figure 1.

2.2. Methodology

2.2.1. Blue-Sky Surface Albedo Estimation

The MODIS, GLASS, and GlobAlbedo land surface albedo products only provide the BSA and WSA, which generally cannot be used to directly compute the surface shortwave net radiation owing to differences in the definitions of various albedo terms. Differences between the BSA and WSA caused by atmospheric effects can be as large as 20% (Manninen et al., 2012). Therefore, we converted them to the blue-sky albedo, $\alpha(\theta,\lambda)$, on the Google Earth Engine (GEE) platform using a linear combination following Wang et al. (2017) and Chrysoulakis et al. (2019):

$$\alpha(\theta,\lambda) = \{1 - S(\theta,\tau(\lambda))\}\,\alpha_{bs}(\theta,\lambda) + S(\theta,\tau(\lambda))\alpha_{ws}(\theta,\lambda), \quad (1)$$

where $\alpha_{bs}(\theta,\lambda)$ is the black-sky albedo, $\alpha_{ws}(\theta,\lambda)$ is the white-sky albedo, $\tau(\lambda)$ is the AOD at 0.55 μm (invalid AOD values were bilinearly interpolated before data processing). $S(\theta,\tau(\lambda))$ is the diffuse skylight ratio, which was retrieved from a LUT based on the solar zenith angle (θ) and τ(λ) (Schaaf et al., 2002).

2.2.2. New Albedo Climatology Generation

Owing to the large data volume and computation resource requirements, we processed the data using Google Earth Engine (GEE) (Gorelick et al., 2017), a cloud-based geospatial processing platform for large-scale environmental monitoring and analysis (Tamiminia et al., 2020), freely providing petabytes of publicly available satellite images, high-speed parallel processing, and a library of Application Programming Interfaces (APIs) that supports JavaScript and Python. The officially published MODIS remote sensing products employed in this study are all included. The daily climatology was calculated by averaging available albedo values of each DOY from 2001 to 2020, separately. After sorting the available samples, the maximum and minimum ones were neglected to constrain the impact of anomalous values, such as extremely high values caused by occasional snowfall in 1 year. Pixels with a large SZA (>75°) were also eliminated to maintain the input data quality (Liu et al., 2009). The snow-free albedo climatology was obtained by ignoring all snow pixels marked by MCD43A2.

The actual and snow-free albedo climatology data were an average of the retrieved values for a given DOY from 2001 to 2020 at the original 500 m scale. The final published datasets also include the albedo climatology data at 0.05° and 0.5° resolutions for modeling convenience: after reprojection from the MODIS sinusoidal projection to Climate Model Grid (CMG) format, we upscaled the outputs from 500 m to 0.05° by calculating the mean value, and 0.5° was aggregated as the 0.05° outcome. Additionally, the global land cover and PFT climatology, generated by selecting the mode at each pixel of MCD12Q1 from 2001 to 2020, were attached. The published data are described in detail in the Data Availability section.

2.2.3. Accuracy Assessment

All albedo climatology data samples of satellite products, reanalysis, and CMIP6 were extracted according to the site locations and paired with ground observations. Taylor diagrams and temporal analysis were used to quantify the absolute accuracy of different datasets at the original spatial resolutions using ground measurements as references (Jia et al., 2018; Yao et al., 2016). The standard deviation (STD), root-mean-square error (RMSE), and correlation coefficient (R) were used as validation indices and are displayed in the Taylor diagrams. The corresponding equations can be found in Taylor (2005). The R and RMSE indicate the overall accuracy, and the STD represents the variability of the albedo samples that should be compared with the STD of the ground measurements. Mean bias was also analyzed and compared. All GCM models were validated at the individual released spatial resolution, whereas the mean CMIP6 was calculated from all GCM data that were bilinearly interpolated to 1°. The new actual climatology data were aggregated to match the spatial resolution of the model data in the spatial comparison section, which was treated as a reference to evaluate the spatial biases of the modeled data both annually and seasonally.

The modeled albedo products have coarse spatial resolutions, which are not suitable for a direct comparison with the site observations at heterogeneous surfaces. Therefore, we calculated a heterogeneity index (HI) to quantify the error caused by the spatial mismatch. It was designed as follows: first, the new climatology was converted to the lat/lon coordinates, aggregated to each modeled scale, and then validated with ground measurements at coarse spatial scales. The difference between RMSE_coarse and RMSE_origin of the new annual climatology represents the relative disturbance of the local heterogeneity (i.e., HI), which can be used to quantify the validation

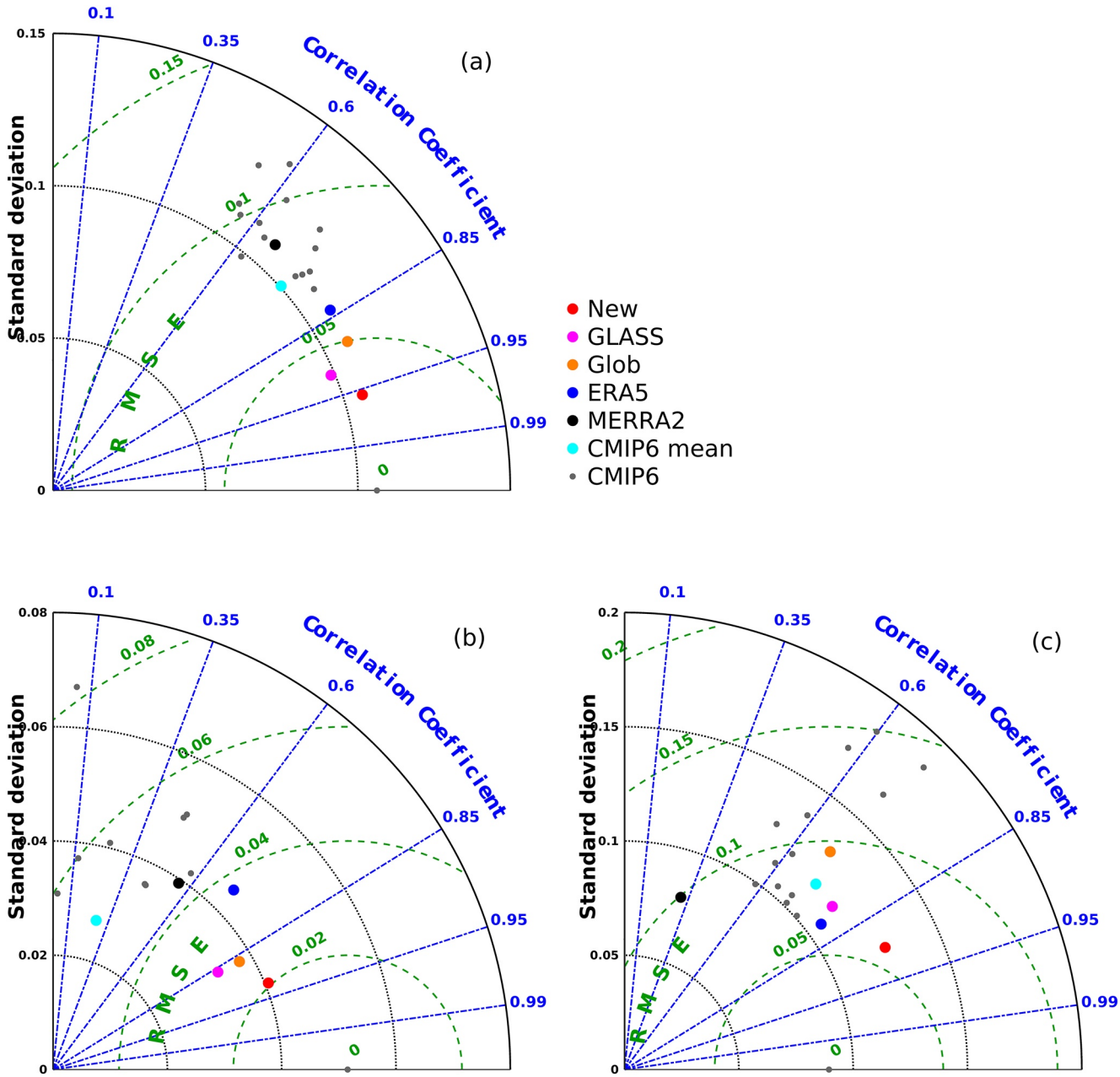

Figure 2. Taylor diagrams of albedo climatology datasets. (a) All available samples, (b) snow-free samples in summer, and (c) snow samples in winter. The black, green, and blue axes represent the standard deviation (STD), root-mean-square error (RMSE), and correlation coefficient (R), respectively.

uncertainty caused by the mismatch of the spatial scale. The HI was then compared with the directly site-quantified accuracy (RMSE) of each model to check if the heterogeneity dominates the data error.

3. Results

3.1. Site Validation

To quantify the accuracy of the new surface albedo climatology, 38 long-term-operating sites belonging to different landcover types were selected (Figure 1). The albedo from the GLASS, GlobAlbedo, reanalysis, and CMIP6 models were extracted and the albedo climatology was calculated. Figure 2 illustrates the accuracies of different albedo climatology datasets. Figure 2a includes all available samples from 38 sites; Figure 2b includes the

snow-free samples of sites in the Northern Hemisphere summer (June–August), indicating the accuracy of the snow-free albedo climatology; and Figure 2c includes snow site samples (albedo >0.45) in the Northern Hemisphere winter (December–February).

Figure 2a indicates that the overall RMSE of the new albedo climatology is 0.031, with a bias of −0.003 and an R of 0.96. The GLASS has an RMSE of 0.042, a bias of 0.005, and R of 0.92; and GlobAlbedo has an RMSE of 0.050, a bias of −0.006, and R of 0.89. Satellite retrieval-based albedo climatology data meet the requirement of climate studies (Li & Garand, 1994) and can be used for model evaluations (Oleson et al., 2003). However, the GLASS and GlobAlbedo have an 8-day temporal resolution that may not be sufficient to characterize the impact of snow cover change (Figure 2c). ERA5 has an RMSE of 0.061, a bias of 0.015, and an R of 0.84, performing better than other reanalysis and model datasets. The HI of ERA5 samples is 0.019, significantly smaller than its RMSE. MERRA2 has an RMSE of 0.087 (bias = −0.021 and HI = 0.024), and CMIP6 albedo climatology datasets are scattered, with accuracies ranging from 0.069 to 0.114 (HI = 0.024–0.031). The RMSE of the mean CMIP6 is 0.074 (bias = −0.032), suggesting that a higher model accuracy can be obtained by averaging multiple models. The CESM2 has the lowest RMSE (0.069) among the CMIP6 models. As the HIs of all model data are very similar, we infer that the major accuracy difference among CMIP6 models is not caused by surface heterogeneity but by the different parameterization schemes.

The validation results of snow-free cases in the summer season (Figure 2b) illustrate that the new albedo climatology performs well for various land cover types (RMSE = 0.021, bias = −0.002, and R = 0.93). GlobAlbedo and GLASS have a comparable accuracy and RMSEs are below 0.03. ERA5 (RMSE = 0.037, R = 0.71, HI = 0.014) is slightly better than MERRA2 (RMSE = 0.044, R = 0.56, HI = 0.018). However, ERA5 shows a larger bias (0.016) in summer. The mean CMIP6 has an RMSE of 0.052 (bias = 0.007 and HI = 0.021) but a small R of 0.28, which indicates that CMIP6 may not capture the snow-free albedo variation caused by land cover (e.g., vegetation coverage). Five models for which R was slightly less than 0 are not included in Figure 2b.

Figure 1c suggests that the new albedo climatology yields better estimate over snow cases (RMSE = 0.055, bias = −0.007, R = 0.91). ERA5 has an RMSE of 0.064 (bias = −0.009 and HI = 0.01), which is better than other satellite, reanalysis, and model datasets. One of the major reasons is that it has a smaller snow albedo bias. The RMSEs of GLASS/GlobAlbedo are 0.072/0.095, and the bias values are 0.013/−0.020. Comparatively, MERRA2 has a larger RMSE of 0.11 with a bias of −0.107. Furthermore, it has a significantly lower STD compared with site measurements, mainly owing to the fact that it underestimates snow albedo values and has a flatter albedo variation in the snow seasons (Figure 3).

The temporal variations of different albedo climatology datasets were also analyzed using the ground truth to elucidate the temporal consistency over two SURFRAD sites, one BSRN site in the Arctic, and one random site representing the clustered European Fluxnet sites (Figure 1). The temporal variation indicates that the new albedo climatology captures the variation in the general pattern and the detailed daily change. The GLASS and GlobAlbedo are in good agreement but have a coarse temporal resolution and cannot reflect detailed variation. Figure 3 also shows that MERRA2 underestimates the albedo climatology, especially during the snow season. ERA5 has good estimation during the snow season, but suffers from systematic overestimation during snow-free seasons.

The site validation results suggest that the new albedo climatology is more accurate than other global datasets from satellite, reanalysis, and CMIP6. ERA5 performs better than other forecasts overall as it better captures the snow albedo variations, while MERRA2 has a clear negative bias for snow cases. Considering the limited number of *in situ* sites, the new albedo climatology offers a reference for assessing global simulated albedo data.

3.2. Spatial Pattern and Comparison

Figure 4 illustrates the spatial patterns of the new albedo climatology under actual and snow-free conditions. The annual mean and mean values in summer and winter are calculated from available climatology values at each pixel. The annual actual albedo climatology maps illustrate that permanently ice-covered regions have an albedo value above 0.8 and no clear temporal variation (Figures 4c and 4e). High-latitude regions and mid-Eurasia in the Northern Hemisphere show a considerable annual temporal variation, which is mainly affected by the snow cover in winter based on the comparison of the albedo patterns of actual (Figure 4e) and snow-free (Figure 4f) climatology. Compared with the actual climatology, the annual snow-free albedo climatology is relatively stable. Furthermore, the boreal region is affected by snow coverage and vegetation phenological phases. The snow-free

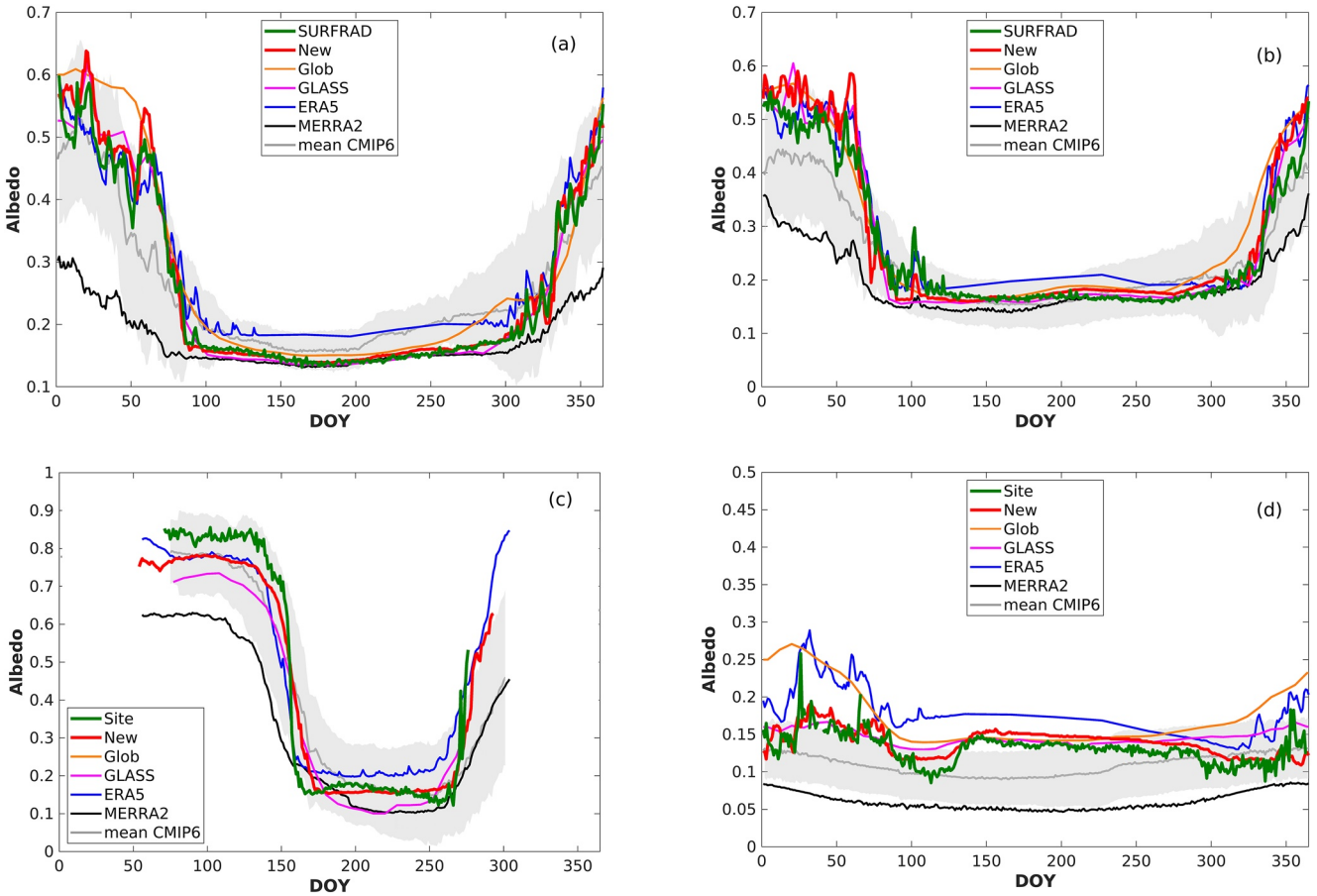

Figure 3. Temporal variations of albedo climatology datasets at different sites. Surface radiation (SURFRAD) (a) FPK and (b) SXF, (c) Baseline Surface Radiation Network BAR, and (d) Fluxnet IT-Col. The gray shadow is the standard deviation of the data series of the 14 Coupled Model Intercomparison Projects Phase 6 models, representing the differences among them.

albedo in these areas slightly increases in winter. The snow-free map in winter left blanks over high latitudes owing to a lack of available valid snow-free albedo values for calculation.

The average observation times on each day from 2001 to 2020 were also mapped to show the global representativeness of the new climatology data and possible uncertainty (Figure 5).

Figure 5a illustrates that the new climatology was generated by a sufficient number of observed records in most areas, whereas fewer observations are available for India, southern China, southern Asia, Western Australia, and tropical forest regions (~10 times). Tropical regions have frequent cloud coverage; thus, the number of observations is smaller. In addition, the MODIS aerosol product contains AOD pixels <0 over Western Australia thus the diffuse skylight ratio cannot be searched from the LUT, which is partially due to AOD retrieval uncertainty over brighter areas (Levy et al., 2013). However, considering that tropical forests and the Australian desert have a stable annual albedo variation, we speculate that the new climatology can capture the albedo characteristics in these regions. In summer, the observations are sufficient for the actual and snow-free albedo. However, in winter the observations over high latitudes are limited, contributing to a possibly larger uncertainty. The RSDS remains low over high-latitude regions in winter, decreasing the uncertainty impact on the surface radiation budget. The observation statistics for each albedo climatology pixel were also attached to the published files.

To demonstrate the superior performance of the new climatology and its potential for improving the albedo accuracy of current state-of-art reanalysis and climate models, a spatial comparison was carried out for which the new climatology was used as a reference (Figure 6).

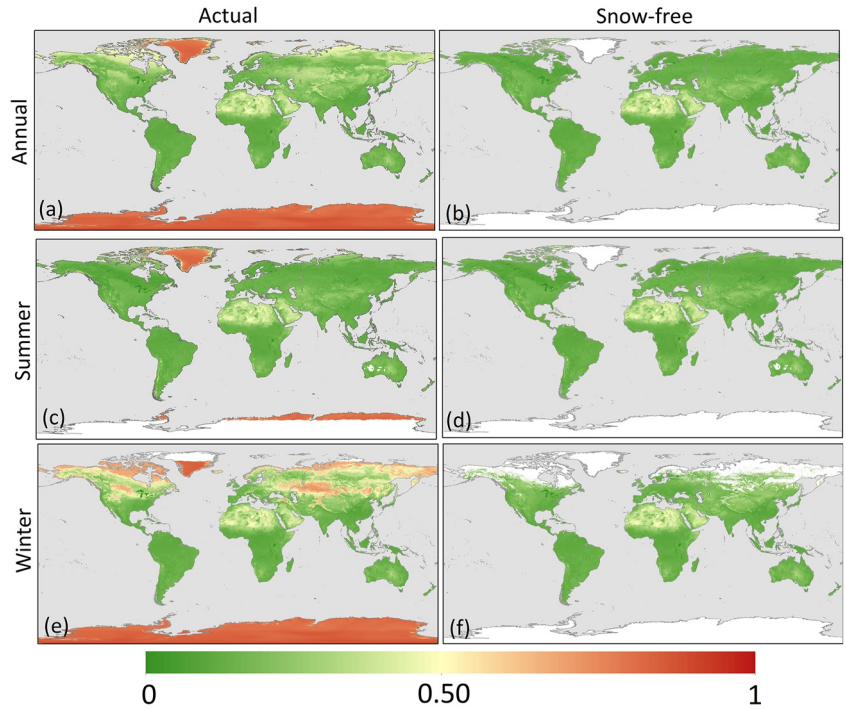

Figure 4. Spatial patterns of the new blue-sky albedo climatology. (a, c, and e) Actual albedo climatology; (b, d, and f) snow-free albedo climatology; (a and b) annual means; (c and d) mean values in summer; (e and f) mean values in winter.

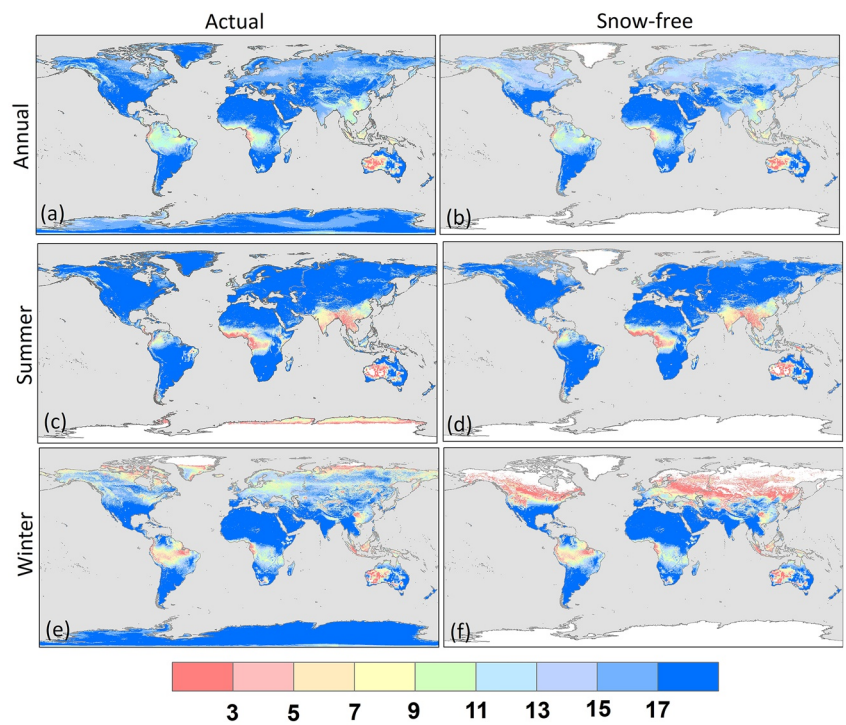

Figure 5. Global patterns of the average observed times from 2001 to 2020. (a, c, and e) Actual albedo climatology; (b, d, and f) snow-free albedo climatology; (a and b) annual means; (c and d) mean values in summer; (e and f) mean values in Winter.

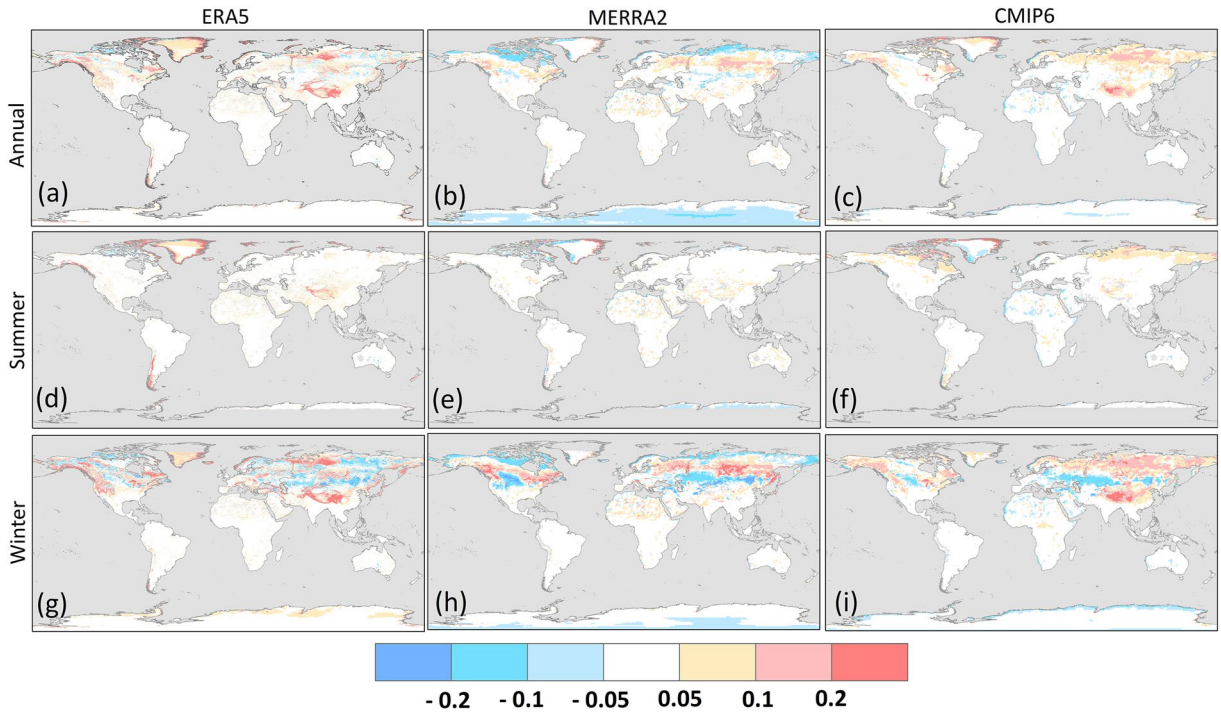

Figure 6. Spatial distribution of the difference between the modeled albedo climatology and new climatology data. (a, d, and g) European Centre for Medium-Range Weather Forecasts Reanalysis 5 (ERA5), (b, e, and j) Modern-Era Retrospective Analysis for Research and Applications Version 2 (MERRA2), (c, f, and i) mean Coupled Model Intercomparison Projects Phase 6 (CMIP6); (a–c) annual difference, (d–f) summer difference, and (g–i) winter difference.

The comparison of the maps at the annual scale shows that ERA5 matches the new climatology better than other gridded albedo climatology data. However, the averaged albedo values over the Tibetan Plateau and Greenland are overestimated (Figures 6a, 6d and 6g), especially in winter. In addition, the differences of all data recorded in winter are larger than those in summer over Eurasia. We infer that this is mainly due to the snow albedo uncertainty. MERRA2 yields significantly underestimated albedo values at high latitudes (Figure 6b), whereas it slightly overestimates the albedo over mid-latitudes and in the Sahara Desert. MERRA2 performs well in the Tibetan Plateau. The CMIP6 overestimates the albedo in the Tibetan Plateau and boreal regions, which is mainly due to the overestimation in winter. Such albedo overestimation in the Tibetan Plateau also occurred in CMIP5 (An et al., 2021). The Weather Research and Forecasting (WRF) model yields a similar overestimation in the Tibetan Plateau, resulting in a cold bias in the surface air temperature simulation, which is mainly due to the simulated precipitation biases and overparameterization of the snow albedo (Meng et al., 2018). Li et al. (2016) analyzed the bias of 37 CMIP5 models with MODIS albedo, and suggested that systematic overestimation occurred during the Northern Hemisphere's winter. The CMIP6 model analysis of this study still shows a similar bias pattern in the winter months (Figure 6i), whereas the bias is limited in summer except for Arctic regions. By employing the RSDS climatology from Clouds and Earth's Radiant Energy Systems (CERES) (Kato et al., 2018; Zhang et al., 2015), we also mapped the corresponding disturbance toward the surface radiation budget (Figure 7) caused by the albedo differences in Figure 6.

Figure 7a indicates that the overestimation of ERA5 over the Tibetan Plateau can cause net radiation (Rn) bias of approximately -30 Wm^{-2} compared with the reference data. The CMIP6 also yields a clear underestimation over the Tibetan Plateau. In addition, the ERA5 Rn at the Greenland edge is $\sim$10 Wm^{-2} lower in summer (Figure 7d). The MERRA2 generally underestimates the albedo in polar regions; thus, Rn is overestimated by $\sim$30 Wm^{-2} in Antarctica (Figure 7h). The calculation of Rn shows that the larger albedo uncertainty over the high northern latitudes has a smaller effect on the surface radiation budget, which is mainly due to the low magnitude of the RSDS, especially in winter.

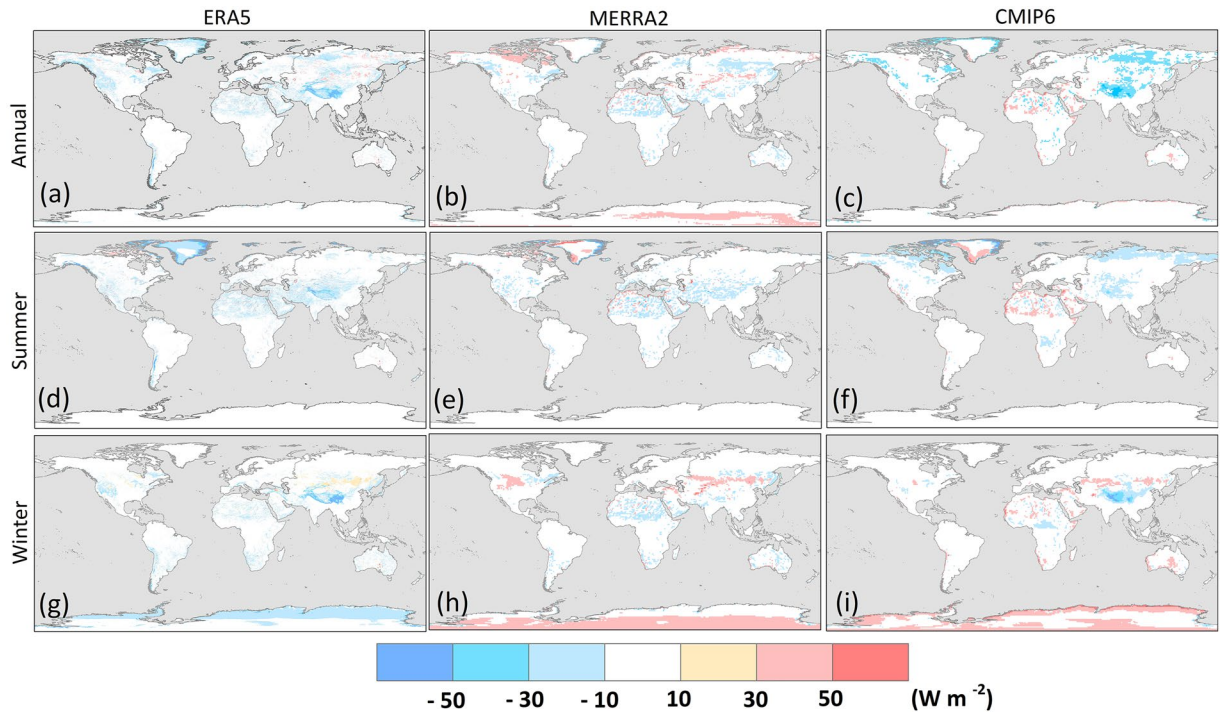

Figure 7. Spatial distribution of net radiation uncertainty caused by the difference between model albedo with the new climatology. (a, d, and g) European Centre for Medium-Range Weather Forecasts Reanalysis 5 (ERA5), (b, e, and j) Modern-Era Retrospective Analysis for Research and Applications Version 2 (MERRA2), (c, f, and i) mean Coupled Model Intercomparison Projects Phase 6 (CMIP6); (a–c) annual difference, (d–f) summer difference, and (g–i) winter difference.

3.3. New Albedo Climatology and PFTs

The albedo climatology of different PFTs reflects the general annual albedo change for each vegetation type at different latitudes, which provides insights into the radiative forcing of different vegetation types and helps to estimate the surface albedo from different land cover types (Gao et al., 2005; He et al., 2014). Therefore, it has been widely utilized to assign albedo values in climate models. In this study, the global climatological albedo variation for different PFTs was analyzed (Figure 8); as the snow cover significantly affects the surface albedo, we also plotted the snow-free albedo variations (right-hand column of Figure 8). Eight PFT types from the MCD12Q1 climatology were employed. To make sure consistency, only pixels that have complete albedo climatology series (365 valid values) were used for calculation.

The updated albedo variations of different PFTs were plotted along the latitude bands and separated by snow conditions. Based on the comparison, snow cover has a considerable effect on the albedo variation of different vegetation types (Atlaskina et al., 2015). The albedo climatology of PFTs in low latitudes remains stable in different seasons. Grass and shrubs (Figures 8f1 and 8e1) have a higher snow albedo than trees (Figures 8a1, 8b1 and 8e1), owing to their low height. Even in the summer, grass and shrubs have higher albedo values because the vegetation coverage is sparser than that of forests. The Northern Hemisphere is more easily affected by snow coverage, as shown in the left-hand column, which is mainly due to the considerably larger land area. The snow-free albedo of different PFTs is shown in the right column. Deciduous needleleaf trees exhibit the largest variation, which is due to the vegetation phenology (Figure 8c2). Grass and crops have a stable annual albedo variation (Figures 8f2 and 8g2), partly because they have relatively lower vegetation coverage. The climatological PFT and land cover maps were also attached to the released data to help users better characterize regional albedo variations of different land cover types.

He et al. (2014) also generated an albedo climatology for different PFTs by using the monthly albedo climatology at a 0.05° spatial scale. However, it is difficult to accurately capture the snow variation with a monthly temporal scale, and mixed pixels might be included in the statistics due to the coarse spatial resolution. Furthermore, the snow disturbance was not removed. Therefore, based on the comparison of the albedo variation of different PFTs obtained in this study with the results in Figure 5 of He et al. (2014), we argue that the daily 500-m blue-sky

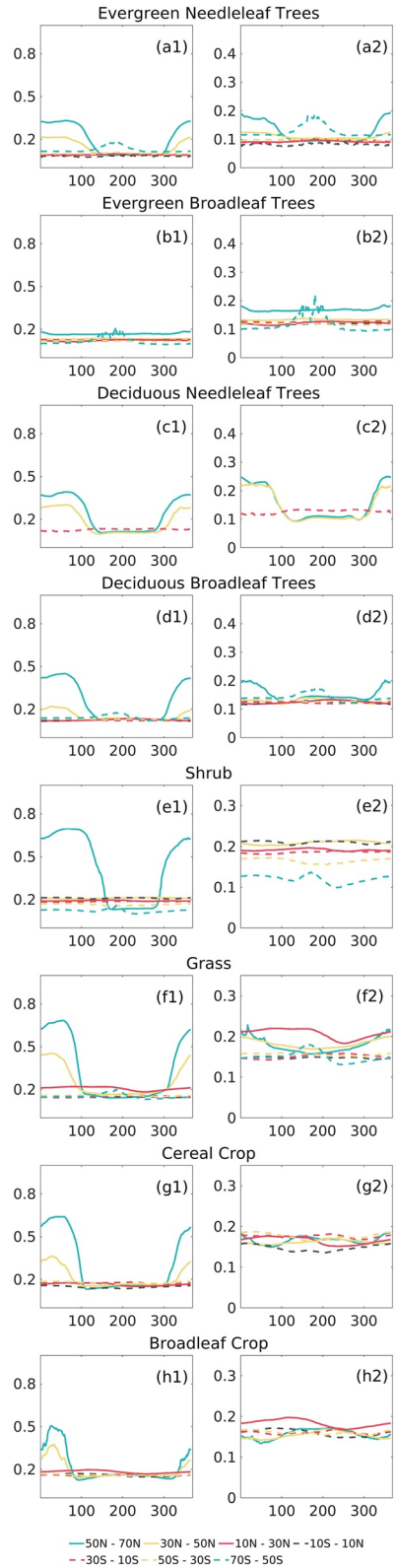

Figure 8. General albedo variations of different Plant Functional Types: (a) Evergreen needleleaf trees, (b) evergreen broadleaf trees, (c) deciduous needleleaf trees, (d) deciduous broadleaf trees, (e) shrubs, (f) grass, (g) cereal crops, (h) broadleaf crops. The left column represents actual climatology conditions; the right column corresponds to snow-free conditions.

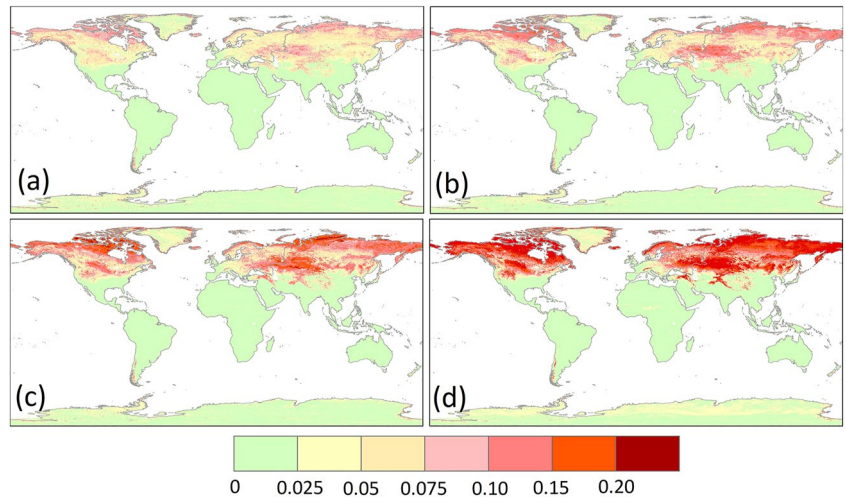

Figure 9. Variability pattern of actual albedo climatology at different temporal resolutions: (a) 8-day; (b) 15-day; (c) monthly; and (d) annual scales.

albedo climatology is more suitable for the characterization of the albedo change of different vegetation types, especially for the determination of the snow effect.

3.4. Variability Analysis

Gao et al. (2014) analyzed the albedo climatology at different spatial resolutions. However, the influence of temporal aggregation remains unclear. This is important especially for the regions with clear snow and non-snow seasons, where coarse temporal resolution may not capture the large albedo variability and causes considerable uncertainty. Therefore, in order to justify the necessity of the albedo climatology at a daily scale, we quantified the temporal variability of the albedo climatology at different temporal scales. The albedo STD represents the temporal variability calculated from the albedo values to be aggregated in each coarser temporal group. For example, 12 albedo groups were obtained by aggregating the daily albedo to the monthly scale (12 months) at each pixel, and there would be 31 albedo values calculating the STD in the first group; finally, the mean of all monthly STDs was then calculated and shown in Figure 9c. The 8-day, 15-day, and monthly scales were selected because they are commonly used in current products. The annual scale was also used to indicate the annual stability of the global albedo.

Figure 9 shows that different temporal resolutions mainly affect areas with clear snow seasons, especially central Eurasia and the boreal tundra. This is because the vegetation types in these two regions are mainly grass, shrubs, and tundra, which have a low height and are easily fully covered by snow. Thus, the albedo dramatically increases in the snow season (Figures 8e1 and 8f1). The 8-day resolution has an albedo variability below 0.1 (most uncertainties are between 0.025 and 0.05; Figure 9a). As the temporal resolution becomes coarser, the albedo variability in central Eurasia and the boreal region increases above 0.2 (Figures 9b and 9c). The albedo in the tropical forest, desert, and permanent snow regions remain stable throughout the year (Figure 9d). The albedo variability analysis illustrates the superiority of the daily scale albedo climatology datasets.

4. Conclusions

Land surface albedo plays a critical role in the surface radiation budget, and is becoming a basic driving factor of climate, hydrological, and biogeochemical modeling, as well as weather forecasting. In many satellite retrievals and climate models, the land surface albedo is generally assigned by LUTs between the albedo and land cover types. However, there are large albedo differences among the modeling predictions, which is partially due to the substantial uncertainty of previously published albedo climatology data. Therefore, precisely mapping global albedo climatology is necessary to better characterize environmental systems. In this study, we generated a new

global surface blue-sky albedo climatology data set based on 20-year MODIS data and carried out comprehensive analyses.

We employed 38 long-term operational sites from the SURFRAD, BSRN, and Fluxnet networks to assess the accuracy of the new actual albedo climatology for different land cover types worldwide. The overall RMSE of the new albedo climatology is 0.031, with a bias of −0.003 and R of 0.96. For snow-free samples in summer, the RMSE is 0.021, bias is −0.002, and R is 0.93, whereas the RMSE, bias, and R for snow albedo are 0.055, −0.007, and 0.91, respectively. The GLASS, GlobAlbedo, ERA5, MERRA2, and 14 CMIP6 modeled albedo climatology datasets were also included for comparison. The results show that the new albedo climatology is superior with respect to absolute accuracy and can be used as a reference for assessing the modeling results. In addition, ERA5 performs better than other modeled and reanalysis datasets because ERA5 better simulated the surface snow albedo, while it results in overestimations during the snow-free season. Both the temporal analysis and bias statistics show that MERRA2 has a clear underestimation for snow albedo. CMIP6 models have various accuracies but most cannot capture albedo changes in detail, especially in the snow-free season.

The new albedo climatology data and corresponding observation times were mapped for different seasons. The actual albedo climatology data were then aggregated and used as references to assess the quality of ERA5, MERRA2, and the average global CMIP6. The results show that ERA5 matches the new climatology better than other models. However, the albedo over the Tibetan Plateau and Greenland is significantly overestimated. CMIP6 also yields overestimations over these regions. MERRA2 underestimates the albedo at high latitudes, whereas it performs well in the Tibetan Plateau. The corresponding disturbance of the albedo uncertainty with respect to the surface net radiation was also quantified.

The general albedo variations of global PFTs were updated based on the new albedo climatology. Grass and shrubs have a higher snow albedo than deciduous needleleaf trees owing to their low height. Snow-free PFTs of albedo were also analyzed. The results indicate that deciduous trees have a larger snow-free albedo variability owing to vegetation phenology.

We quantified the global albedo variability pattern using the new albedo climatology at different temporal resolutions. The results illustrate that coarser temporal resolutions mainly affect areas with snow seasons, especially central Eurasia and the boreal region. The 8-day resolution has albedo variabilities ranging from 0.025 to 0.05. As the temporal resolution becomes coarser, the variabilities in central Eurasia and the boreal region can reach values above 0.2. The annual pattern also indicates that the Southern Hemisphere has a more stable albedo variation owing to the smaller variation in the snow coverage.

We published a new global daily blue-sky albedo climatology data set, which has the potential to improve the accuracies of model prediction and satellite retrievals by data assimilation, and it also provides a reliable ground reference for model assessment. In the future, we would like to combine the albedo clear-sky retrieval product with new climatology datasets to generate a global all-sky albedo product.

Conflict of Interest

The authors declare no conflicts of interest relevant to this study.

Data Availability Statement

The daily 500-m global surface blue-sky albedo climatology data set is freely available at https://doi.org/10.5281/zenodo.6359686 (Jia et al., 2021a). It utilizes the basic Moderate Resolution Imaging Spectroradiometer (MODIS) product format with a sinusoidal projection. After reprojection and aggregation, the global Climate Modeling Grid (CMG) albedo climatology datasets at 0.05° and 0.5° resolutions are available at https://doi.org/10.5281/zenodo.6350821 (Jia et al., 2021b). The full data set is also accessible at the University of Maryland (http://glass.umd.edu/albedo_clim/). All published datasets include actual and snow-free blue-sky albedo climatology data. In addition, the corresponding observation times for each climatology grid were attached as quality marks. For application convenience, the International Geosphere-Biosphere Programme and plant functional type climatologies (from 2001 to 2020) of the MODIS product (MCD12Q1) were also generated and attached at each spatial

resolution. To demonstrate the heterogeneity of the land cover climatology, the percentage of the dominant type in each aggregation group was calculated.

Acknowledgments
This study was supported by the National Oceanic and Atmospheric Administration (NOAA) Suomi-NPP/Visible Infrared Imaging Radiometer Suite (VIIRS) albedo project. The scientific results and conclusions as well as any views or opinions expressed herein are those of the authors and do not necessarily reflect those of NOAA or the Department of Commerce. The authors gratefully acknowledge Google Earth Engine for providing the data and computation platform and Zenodo for publishing the product. We also thank the European Centre for Medium-Range Weather Forecasts (ECMWF) Center for providing ECMWF Reanalysis 5 reanalysis data, Global Modeling and Assimilation Office for providing Modern-Era Retrospective Analysis for Research and Applications Version 2, and the World Climate Research Programme for providing Coupled Model Intercomparison Projects Phase 6 data. We acknowledge the Surface Radiation and Baseline Surface Radiation Network for providing field measurements of flux variables. We also thank Zhihao Wang and Zina Mitraka for discussions about technical issues.

References

An, Y., Meng, X., Zhao, L., Li, Z., Wang, S., Shang, L., et al. (2021). Evaluation of surface albedo over the Tibetan Plateau simulated by CMIP5 models using in-situ measurements and MODIS. *International Journal of Climatology*, *42*(2), 928–951. https://doi.org/10.1002/joc.7281

Asner, G. P., Wessman, C. A., Schimel, D. S., & Archer, S. (1998). Variability in leaf and litter optical properties: Implications for BRDF model inversions using AVHRR, MODIS, and MISR. *Remote Sensing of Environment*, *63*(3), 243–257. https://doi.org/10.1016/s0034-4257(97)00138-7

Atlaskina, K., Berninger, F., & Leeuw, G. d. (2015). Satellite observations of changes in snow-covered land surface albedo during spring in the Northern Hemisphere. *The Cryosphere*, *9*(5), 1879–1893. https://doi.org/10.5194/tc-9-1879-2015

Augustine, J. A., DeLuisi, J. J., & Long, C. N. (2000). SURFRAD—A national surface radiation budget network for atmospheric research. *Bulletin of the American Meteorological Society*, *81*(10), 2341–2357. https://doi.org/10.1175/1520-0477(2000)081<2341:sansrb>2.3.co

Barnsley, M., Quaife, T., Hobson, P., Shaw, J., Lewis, P., Disney, M., et al. (2000). Estimation of land-surface albedo and biophysical properties using SPOT-4 VGT and semi-empirical BRDF models. In *Paper presented at Proceedings of International SPOT4 Vegetation Conference*. Stolkholm.

Boussetta, S., Balsamo, G., Dutra, E., Beljaars, A., & Albergel, C. (2015). Assimilation of surface albedo and vegetation states from satellite observations and their impact on numerical weather prediction. *Remote Sensing of Environment*, *163*, 111–126. https://doi.org/10.1016/j.rse.2015.03.009

Burakowski, E., Tawfik, A., Ouimette, A., Lepine, L., Novick, K., Ollinger, S., et al. (2018). The role of surface roughness, albedo, and Bowen ratio on ecosystem energy balance in the Eastern United States. *Agricultural and Forest Meteorology*, *249*, 367–376. https://doi.org/10.1016/j.agrformet.2017.11.030

Cao, J., Wang, B., Yang, Y.-M., Ma, L., Li, J., Sun, B., et al. (2018). The NUIST Earth system model (NESM) version 3: Description and preliminary evaluation. *Geoscientific Model Development*, *11*(7), 2975–2993. https://doi.org/10.5194/gmd-11-2975-2018

Carrer, D., Meurey, C., Ceamanos, X., Roujean, J.-L., Calvet, J.-C., & Liu, S. (2014). Dynamic mapping of snow-free vegetation and bare soil albedos at global 1 km scale from 10-year analysis of MODIS satellite products. *Remote Sensing of Environment*, *140*, 420–432. https://doi.org/10.1016/j.rse.2013.08.041

Cescatti, A., Marcolla, B., Vannan, S. K. S., Pan, J. Y., Román, M. O., Yang, X., et al. (2012). Intercomparison of MODIS albedo retrievals and in situ measurements across the global FLUXNET network. *Remote Sensing of Environment*, *121*, 323–334. https://doi.org/10.1016/j.rse.2012.02.019

Chou, M. D., & Suarez, M. J. (1999). A solar radiation parameterization for atmospheric studies, NASA TM-104606. *National Aeronautics and Space Administration Technical Memorandum*, *15*, 44.

Chrysoulakis, N., Mitraka, Z., & Gorelick, N. (2019). Exploiting satellite observations for global surface albedo trends monitoring. *Theoretical and Applied Climatology*, *137*(1–2), 1171–1179. https://doi.org/10.1007/s00704-018-2663-6

Cui, T., Li, C., & Tian, F. (2021). Evaluation of temperature and precipitation simulations in CMIP6 models over the Tibetan Plateau. *Earth and Space Science*, e2020EA001620. https://doi.org/10.1029/2020ea001620

Cullather, R. I., & Bosilovich, M. G. (2012). The energy budget of the polar atmosphere in MERRA. *Journal of Climate*, *25*(1), 5–24. https://doi.org/10.1175/2011jcli4138.1

Danabasoglu, G., Lamarque, J. F., Bacmeister, J., Bailey, D., DuVivier, A., Edwards, J., et al. (2020). The community Earth system model version 2 (CESM2). *Journal of Advances in Modeling Earth Systems*, *12*(2). https://doi.org/10.1029/2019ms001916

Danabasoglu, G., Lawrence, D., Lindsay, K., Lipscomb, W., & Strand, G. (2019). *NCAR CESM2 model output prepared for CMIP6 CMIP historical*. Earth System Grid Federation, Version, 20190912. 485.

Dickinson, R. E. (1995). Land processes in climate models. *Remote Sensing of Environment*, *51*(1), 27–38. https://doi.org/10.1016/0034-4257(94)00062-r

Di Napoli, C., Barnard, C., Prudhomme, C., Cloke, H. L., & Pappenberger, F. (2020). ERA5-HEAT: A global gridded historical dataset of human thermal comfort indices from climate reanalysis. *Geoscience Data Journal*. https://doi.org/10.1002/gdj3.102

Dorman, J., & Sellers, P. J. (1989). A global climatology of albedo, roughness length and stomatal resistance for atmospheric general circulation models as represented by the simple biosphere model (SiB). *Journal of Applied Meteorology and Climatology*, *28*(9), 833–855. https://doi.org/10.1175/1520-0450(1989)028<0833:agcoar>2.0.co;2

Driemel, A., Augustine, J., Behrens, K., Colle, S., Cox, C., Cuevas-Agulló, E., et al. (2018). Baseline surface radiation network (BSRN): Structure and data description (1992–2017). *Earth System Science Data*, *10*(3), 1491–1501. https://doi.org/10.5194/essd-10-1491-2018

Gao, F., He, T., Wang, Z., Ghimire, B., Shuai, Y., Masek, J. G., et al. (2014). Multiscale climatological albedo look-up maps derived from Moderate Resolution Imaging Spectroradiometer BRDF/albedo products. *Journal of Applied Remote Sensing*, *8*(1), 083532. https://doi.org/10.1117/1.jrs.8.083532

Gao, F., Schaaf, C. B., Strahler, A. H., Roesch, A., Lucht, W., & Dickinson, R. (2005). MODIS bidirectional reflectance distribution function and albedo Climate Modeling Grid products and the variability of albedo for major global vegetation types. *Journal of Geophysical Research*, *110*(D1). https://doi.org/10.1029/2004jd005190

GCOS, O. (2004). *Implementation plan for the global observing system for climate in support of the UNFCCC*. GCOS-92.

Geiger, B., Carrer, D., Franchisteguy, L., Roujean, J.-L., & Meurey, C. (2008). Land surface albedo derived on a daily basis from Meteosat Second Generation observations. *IEEE Transactions on Geoscience and Remote Sensing*, *46*(11), 3841–3856. https://doi.org/10.1109/tgrs.2008.2001798

Gorelick, N., Hancher, M., Dixon, M., Ilyushchenko, S., Thau, D., & Moore, R. (2017). Google Earth Engine: Planetary-scale geospatial analysis for everyone. *Remote Sensing of Environment*, *202*, 18–27. https://doi.org/10.1016/j.rse.2017.06.031

Graversen, R. G., & Wang, M. (2009). Polar amplification in a coupled climate model with locked albedo. *Climate Dynamics*, *33*(5), 629–643. https://doi.org/10.1007/s00382-009-0535-6

Grey, W. M. F., Houldcroft, C. J., Barnsley, M., Taylor, C. M., Los, S. O., & North, P. R. J. (2009). New vegetation Albedo parameters and global fields of soil background Albedo derived from MODIS for use in a climate model. *Journal of Hydrometeorology*, *10*(1), 183–198. https://doi.org/10.1175/2008jhm1021.1

He, B., Bao, Q., Wang, X., Zhou, L., Wu, X., Liu, Y., et al. (2019). CAS FGOALS-f3-L model datasets for CMIP6 historical atmospheric model Intercomparison project simulation. *Advances in Atmospheric Sciences*, *36*(8), 771–778. https://doi.org/10.1007/s00376-019-9027-8

He, T., Liang, S., & Song, D. X. (2014). Analysis of global land surface albedo climatology and spatial-temporal variation during 1981–2010 from multiple satellite products. *Journal of Geophysical Research: Atmospheres*, *119*(17), 10–281. https://doi.org/10.1002/2014jd021667

He, T., Liang, S., Wang, D., Wu, H., Yu, Y., & Wang, J. (2012). Estimation of surface albedo and directional reflectance from Moderate Resolution Imaging Spectroradiometer (MODIS) observations. *Remote Sensing of Environment*, *119*, 286–300. https://doi.org/10.1016/j.rse.2012.01.004

Hersbach, H., Bell, B., Berrisford, P., Hirahara, S., Horányi, A., Muñoz-Sabater, J., et al. (2020). The ERA5 global reanalysis. *Quarterly Journal of the Royal Meteorological Society*, *146*(730), 1999–2049. https://doi.org/10.1002/qj.3803

Hinkelman, L. M. (2019). The global radiative energy budget in MERRA and MERRA-2: Evaluation with respect to CERES EBAF data. *Journal of Climate*, *32*(6), 1973–1994. https://doi.org/10.1175/jcli-d-18-0445.1

Houldcroft, C. J., Grey, W. M., Barnsley, M., Taylor, C. M., Los, S. O., & North, P. R. (2009). New vegetation albedo parameters and global fields of soil background albedo derived from MODIS for use in a climate model. *Journal of Hydrometeorology*, *10*(1), 183–198. https://doi.org/10.1175/2008jhm1021.1

Jia, A., Liang, S., Jiang, B., Zhang, X., & Wang, G. (2018). Comprehensive assessment of global surface net radiation products and uncertainty analysis. *Journal of Geophysical Research: Atmospheres*, *123*(4), 1970–1989. https://doi.org/10.1002/2017jd027903

Jia, A., Ma, H., Liang, S., & Wang, D. (2021). Cloudy-sky land surface temperature from VIIRS and MODIS satellite data using a surface energy balance-based method. *Remote Sensing of Environment*, *263*, 112566. https://doi.org/10.1016/j.rse.2021.112566

Jia, A., Wang, D., Liang, S., Peng, J., & Yu, Y. (2021a). *Global daily surface blue-sky albedo climatology and land cover climatology dataset from 20-year MODIS products (500m)*. Zenodo. https://doi.org/10.5281/zenodo.6359686

Jia, A., Wang, D., Liang, S., Peng, J., & Yu, Y. (2021b). *Global daily surface blue-sky albedo climatology and land cover climatology dataset from 20-year MODIS products (CMG)*. Zenodo. https://doi.org/10.5281/zenodo.6350821

Jian, B., Li, J., Zhao, Y., He, Y., Wang, J., & Huang, J. (2020). Evaluation of the CMIP6 planetary albedo climatology using satellite observations. *Climate Dynamics*, *54*(11–12), 5145–5161. https://doi.org/10.1007/s00382-020-05277-4

Karlsson, K.-G., Riihelä, A., Müller, R., Meirink, J., Sedlar, J., Stengel, M., et al. (2013). CLARA-A1: A cloud, albedo, and radiation dataset from 28 yr of global AVHRR data. *Atmospheric Chemistry and Physics*, *13*(10), 5351–5367. https://doi.org/10.5194/acp-13-5351-2013

Kato, S., Rose, F. G., Rutan, D. A., Thorsen, T. J., Loeb, N. G., Doelling, D. R., et al. (2018). Surface irradiances of edition 4.0 clouds and the Earth's radiant energy system (CERES) energy balanced and filled (EBAF) data product. *Journal of Climate*, *31*(11), 4501–4527. https://doi.org/10.1175/jcli-d-17-0523.1

Kim, Y. H., Pak, G., Noh, Y., Lee, M.-I., Yeh, S.-W., Kim, D., et al. (2020). Korea institute of ocean science & technology Earth system model and its simulation characteristics. In *Paper Presented at EGU General Assembly Conference Abstracts*.

Lawrence, D., Fisher, R., Koven, C., Oleson, K., Swenson, S., & Vertenstein, M. (2020). *CLM5 documentation*.

Lawrence, D., Fisher, R. A., Koven, C. D., Oleson, K. W., Swenson, S. C., Bonan, G., et al. (2019). The Community Land Model version 5: Description of new features, benchmarking, and impact of forcing uncertainty. *Journal of Advances in Modeling Earth Systems*, *11*(12), 4245–4287. https://doi.org/10.1029/2018ms001583

Lawrence, P. J., & Chase, T. N. (2007). Representing a new MODIS consistent land surface in the Community Land Model (CLM 3.0). *Journal of Geophysical Research*, *112*(G1). https://doi.org/10.1029/2006jg000168

Levine, X. J., & Boos, W. R. (2017). Land surface albedo bias in climate models and its association with tropical rainfall. *Geophysical Research Letters*, *44*(12), 6363–6372. https://doi.org/10.1002/2017gl072510

Levy, R., Mattoo, S., Munchak, L., Remer, L., Sayer, A., Patadia, F., & Hsu, N. (2013). The Collection 6 MODIS aerosol products over land and ocean. *Atmospheric Measurement Techniques*, *6*(11), 2989–3034. https://doi.org/10.5194/amt-6-2989-2013

Lewis, P., Guanter, L., Saldana, G. L., Muller, J.-P., Watson, G., Shane, N., et al. (2012). The ESA globAlbedo project: Algorithm. In *Paper Presented at 2012 IEEE International Geoscience and Remote Sensing Symposium, IEEE*.

Li, J., Miao, C., Wei, W., Zhang, G., Hua, L., Chen, Y., & Wang, X. (2021). Evaluation of CMIP6 global climate models for simulating land surface energy and water fluxes during 1979–2014. *Journal of Advances in Modeling Earth Systems*, *13*(6). https://doi.org/10.1029/2021ms002515

Li, L., Yu, Y., Tang, Y., Lin, P., Xie, J., Song, M., et al. (2020). The flexible global ocean-atmosphere-land system model grid-point version 3 (fgoals-g3): Description and evaluation. *Journal of Advances in Modeling Earth Systems*, *12*(9), e2019MS002012. https://doi.org/10.1029/2019ms002012

Li, Y., Wang, T., Zeng, Z., Peng, S., Lian, X., & Piao, S. (2016). Evaluating biases in simulated land surface albedo from CMIP5 global climate models. *Journal of Geophysical Research: Atmospheres*, *121*(11), 6178–6190. https://doi.org/10.1002/2016jd024774

Li, Z., & Garand, L. (1994). Estimation of surface albedo from space: A parameterization for global application. *Journal of Geophysical Research*, *99*(D4), 8335–8350. https://doi.org/10.1029/94jd00225

Li, Z.-L., Tang, B.-H., Wu, H., Ren, H., Yan, G., Wan, Z., et al. (2013). Satellite-derived land surface temperature: Current status and perspectives. *Remote Sensing of Environment*, *131*, 14–37. https://doi.org/10.1016/j.rse.2012.12.008

Liang, S., Cheng, J., Jia, K., Jiang, B., Liu, Q., Xiao, Z., et al. (2021). The global land surface satellite (GLASS) product suite. *Bulletin of the American Meteorological Society*, *102*(2), E323–E337. https://doi.org/10.1175/bams-d-18-0341.1

Liang, S., Wang, K. C., Zhang, X. T., & Wild, M. (2010). Review on estimation of land surface radiation and energy budgets from ground measurement, remote sensing and model simulations. *IEEE Journal of Selected Topics in Applied Earth Observations and Remote Sensing*, *3*(3), 225–240. https://doi.org/10.1109/Jstars.2010.2048556

Liang, S., Zhao, X., Liu, S., Yuan, W., Cheng, X., Xiao, Z., et al. (2013). A long-term global land surface satellite (GLASS) data-set for environmental studies. *International Journal of Digital Earth*, *6*(1), 5–33. https://doi.org/10.1080/17538947.2013.805262

Liu, J., Schaaf, C., Strahler, A., Jiao, Z., Shuai, Y., Zhang, Q., et al. (2009). Validation of Moderate Resolution Imaging Spectroradiometer (MODIS) albedo retrieval algorithm: Dependence of albedo on solar zenith angle. *Journal of Geophysical Research*, *114*(D1). https://doi.org/10.1029/2008jd009969

Liu, Q., Wang, L., Qu, Y., Liu, N., Liu, S., Tang, H., & Liang, S. (2013). Preliminary evaluation of the long-term GLASS albedo product. *International Journal of Digital Earth*, *6*(1), 69–95. https://doi.org/10.1080/17538947.2013.804601

Lucht, W., Schaaf, C. B., & Strahler, A. H. (2000). An algorithm for the retrieval of albedo from space using semiempirical BRDF models. *IEEE Transactions on Geoscience and Remote Sensing*, *38*(2), 977–998. https://doi.org/10.1109/36.841980

Lupu, C., & Geer, A. J. (2015). *Operational implementation of RTTOV-11 in the IFS*. European Centre for Medium-Range Weather Forecasts.

Manninen, T., Riihelä, A., & Leeuw, G. d. (2012). Atmospheric effect on the ground-based measurements of broadband surface albedo. *Atmospheric Measurement Techniques*, *5*(11), 2675–2688. https://doi.org/10.5194/amt-5-2675-2012

Masson, V., Le Moigne, P., Martin, E., Faroux, S., Alias, A., Alkama, R., et al. (2013). The SURFEXv7.2 land and ocean surface platform for coupled or offline simulation of Earth surface variables and fluxes. *Geoscientific Model Development*, *6*(4), 929–960. https://doi.org/10.5194/gmd-6-929-2013

Meng, X., Lyu, S., Zhang, T., Zhao, L., Li, Z., Han, B., et al. (2018). Simulated cold bias being improved by using MODIS time-varying albedo in the Tibetan Plateau in WRF model. *Environmental Research Letters*, *13*(4), 044028. https://doi.org/10.1088/1748-9326/aab44a

Molod, A., Takacs, L., Suarez, M., & Bacmeister, J. (2015). Development of the GEOS-5 atmospheric general circulation model: Evolution from MERRA to MERRA2. *Geoscientific Model Development*, *8*(5), 1339–1356. https://doi.org/10.5194/gmd-8-1339-2015

Moody, E. G., King, M. D., Platnick, S., Schaaf, C. B., & Gao, F. (2005). Spatially complete global spectral surface albedos: Value-added datasets derived from Terra MODIS land products. *IEEE Transactions on Geoscience and Remote Sensing*, *43*(1), 144–158. https://doi.org/10.1109/tgrs.2004.838359

Morcrette, J., Barker, H. W., Cole, J., Iacono, M. J., & Pincus, R. (2008). Impact of a new radiation package, McRad, in the ECMWF integrated forecasting system. *Monthly Weather Review*, *136*(12), 4773–4798. https://doi.org/10.1175/2008mwr2363.1

Muller, J.-P. (2013). *GlobAlbedo final validation reportRep*. University College London.

Muller, J.-P., López, G., Watson, G., Shane, N., Kennedy, T., Yuen, P., et al. (2012). The ESA GlobAlbedo Project for mapping the Earth's land surface albedo for 15 years from European sensors. In *Paper Presented at Geophysical Research Abstracts*.

Muñoz-Sabater, J., Dutra, E., Agustí-Panareda, A., Albergel, C., Arduini, G., Balsamo, G., et al. (2021). ERA5-Land: A state-of-the-art global reanalysis dataset for land applications. *Earth System Science Data*, *13*(9), 4349–4383.

Oleson, K. W., Bonan, G. B., Schaaf, C., Gao, F., Jin, Y., & Strahler, A. (2003). Assessment of global climate model land surface albedo using MODIS data. *Geophysical Research Letters*, *30*(8). https://doi.org/10.1029/2002gl016749

Park, S., Shin, J., Kim, S., Oh, E., & Kim, Y. (2019). Global climate simulated by the Seoul National University atmosphere model version 0 with a unified convection scheme (SAM0-UNICON). *Journal of Climate*, *32*(10), 2917–2949. https://doi.org/10.1175/jcli-d-18-0796.1

Platnick, S., King, M., Meyer, K., Wind, G., Amarasinghe, N., Marchant, B., et al. (2015). *MODIS atmosphere L3 monthly product, NASA MODIS Adaptive Processing System*. Goddard Space Flight Center.20.

Qu, Y., Liang, S. L., Liu, Q., He, T., Liu, S. H., & Li, X. W. (2015). Mapping surface broadband albedo from satellite Observations: A review of literature on algorithms and products. *Remote Sensing*, *7*(1), 990–1020. https://doi.org/10.3390/rs70100990

Qu, Y., Liu, Q., Liang, S., Wang, L., Liu, N., & Liu, S. (2014). Direct-estimation algorithm for mapping daily land-surface broadband albedo from MODIS data. *IEEE Transactions on Geoscience and Remote Sensing*, *52*(2), 907–919. https://doi.org/10.1109/tgrs.2013.2245670

Roesch, A., Wild, M., Ohmura, A., Dutton, E. G., Long, C. N., & Zhang, T. (2011). Corrigendum to "Assessment of BSRN radiation records for the computation of monthly means" published in Atmos. Meas. Tech., 4, 339–354, 2011. *Atmospheric Measurement Techniques & Discussions*, *4*(2), 975–1018. https://doi.org/10.5194/amt-4-339-2011

Rutan, D., Kato, S., Doelling, D. R., Rose, F. G., Nguyen, L. T., Caldwell, T. E., & Loeb, N. G. (2015). CERES synoptic product: Methodology and validation of surface radiant flux. *Journal of Atmospheric and Oceanic Technology*, *32*(6), 1121–1143. https://doi.org/10.1175/jtech-d-14-00165.1

Rutan, D., Rose, F., Roman, M., Manalo-Smith, N., Schaaf, C., & Charlock, T. (2009). Development and assessment of broadband surface albedo from clouds and the Earth's radiant energy system clouds and radiation Swath data product. *Journal of Geophysical Research*, *114*(D8). https://doi.org/10.1029/2008jd010669

Schaaf, C., Gao, F., Strahler, A. H., Lucht, W., Li, X., Tsang, T., et al. (2002). First operational BRDF, albedo nadir reflectance products from MODIS. *Remote Sensing of Environment*, *83*(1–2), 135–148. https://doi.org/10.1016/s0034-4257(02)00091-3

Schaaf, C., Liu, J., Gao, F., & Strahler, A. H. (2011). MODIS albedo and reflectance anisotropy products from Aqua and Terra. *Land Remote Sensing and Global Environmental Change: NASA's Earth Observing System and the Science of ASTER and MODIS*, *11*, 549–561.

Schaaf, C., & Wang, Z. (2015a). MCD43A2 MODIS/Terra+ Aqua BRDF/albedo quality daily L3 global–500m V006 [Data set]. NASA EOSDIS Land Processes DAAC. https://doi.org/10.5067/MODIS/MCD43A2.006

Schaaf, C., & Wang, Z. (2015b). MCD43A3 MODIS/Terra+ Aqua BRDF/albedo daily L3 global– 500m V006 [Data set]. NASA EOSDIS Land Processes DAAC. https://doi.org/10.5067/MODIS/MCD43A3.006

Shu, Q., Wang, Q., Song, Z., Qiao, F., Zhao, J., Chu, M., & Li, X. (2020). Assessment of sea ice extent in CMIP6 with comparison to observations and CMIP5. *Geophysical Research Letters*, *47*(9), e2020GL087965. https://doi.org/10.1029/2020gl087965

Strahler, A. H., Muller, J., Lucht, W., Schaaf, C., Tsang, T., Gao, F., et al. (1999). MODIS BRDF/albedo product: Algorithm theoretical basis document version 5.0. *MODIS documentation*, *23*(4), 42–47.

Stroeve, J., Box, J. E., Gao, F., Liang, S., Nolin, A., & Schaaf, C. (2005). Accuracy assessment of the MODIS 16-day albedo product for snow: Comparisons with Greenland in situ measurements. *Remote Sensing of Environment*, *94*(1), 46–60. https://doi.org/10.1016/j.rse.2004.09.001

Suarez, M. J., & Chou, M. D. (1994). An efficient thermal infrared radiation parameterization for use in general circulation models. In *Paper Presented at Global Modeling And Data Assimilation, Technical Memorandum 104606*. Goddard Space Flight Center. 102. https://doi.org/10.4236/ajcc.2015.41006

Sulla-Menashe, D., & Friedl, M. A. (2018). *User guide to collection 6 MODIS land cover (MCD12Q1 and MCD12C1) product* (pp. 1–18). USGS.

Swart, N. C., Cole, J. N., Kharin, V. V., Lazare, M., Scinocca, J. F., Gillett, N. P., et al. (2019). The Canadian Earth System Model Version 5 (CanESM5. 0.3). *Geoscientific Model Development*, *12*(11), 4823–4873. https://doi.org/10.5194/gmd-12-4823-2019

Tamiminia, H., Salehi, B., Mahdianpari, M., Quackenbush, L., Adeli, S., & Brisco, B. (2020). Google Earth engine for geo-big data applications: A meta-analysis and systematic review. *ISPRS Journal of Photogrammetry and Remote Sensing*, *164*, 152–170. https://doi.org/10.1016/j.isprsjprs.2020.04.001

Tatebe, H., Ogura, T., Nitta, T., Komuro, Y., Ogochi, K., Takemura, T., et al. (2019). Description and basic evaluation of simulated mean state, internal variability, and climate sensitivity in MIROC6. *Geoscientific Model Development*, *12*(7), 2727–2765. https://doi.org/10.5194/gmd-12-2727-2019

Taylor, K. E. (2005). *Taylor diagram primer* (pp. 1–4). Pap. https://doi.org/10.1057/9780230505650_1

Thackeray, C. W., Fletcher, C. G., & Derksen, C. (2019). Diagnosing the impacts of Northern Hemisphere surface albedo biases on simulated climate. *Journal of Climate*, *32*(6), 1777–1795. https://doi.org/10.1175/jcli-d-18-0083.1

Van Angelen, J., Lenaerts, J., Lhermitte, S., Fettweis, X., Kuipers Munneke, P., Van den Broeke, M., et al. (2012). Sensitivity of Greenland ice Sheet surface mass balance to surface albedo parameterization: A study with a regional climate model. *The Cryosphere*, *6*(5), 1175–1186. https://doi.org/10.5194/tc-6-1175-2012

Vignesh, P. P., Jiang, J. H., Kishore, P., Su, H., Smay, T., Brighton, N., & Velicogna, I. (2020). Assessment of CMIP6 cloud fraction and comparison with satellite observations. *Earth and Space Science*, *7*(2), e2019EA000975. https://doi.org/10.1029/2019ea000975

Wang, D., Liang, S., He, T., & Yu, Y. (2013). Direct estimation of land surface albedo from VIIRS data: Algorithm improvement and preliminary validation. *Journal of Geophysical Research: Atmospheres*, *118*(22), 12–577. https://doi.org/10.1002/2013jd020417

Wang, D., Liang, S., He, T., Yu, Y., Schaaf, C., & Wang, Z. (2015). Estimating daily mean land surface albedo from MODIS data. *Journal of Geophysical Research: Atmospheres*, *120*(10), 4825–4841. https://doi.org/10.1002/2015jd023178

Wang, D., Liang, S., Zhang, Y., Gao, X., Brown, M. G., & Jia, A. (2020). A new set of MODIS land products (MCD18): Downward shortwave radiation and photosynthetically active radiation. *Remote Sensing*, *12*(1), 168. https://doi.org/10.3390/rs12010168

Wang, D., Liang, S., Zhou, Y., He, T., & Yu, Y. (2016). A new method for retrieving daily land surface albedo from VIIRS data. *IEEE Transactions on Geoscience and Remote Sensing*, *55*(3), 1765–1775.

Wang, D., Liang, S., Zhou, Y., He, T., & Yu, Y. (2017). A new method for retrieving daily land surface albedo from VIIRS data. *IEEE Transactions on Geoscience and Remote Sensing*, *55*(3), 1765–1775. https://doi.org/10.1109/tgrs.2016.2632624

Wang, K., & Dickinson, R. E. (2013). Global atmospheric downward longwave radiation at the surface from ground-based observations, satellite retrievals, and reanalyses. *Reviews of Geophysics*, *51*(2), 150–185. https://doi.org/10.1002/rog.20009

Wang, K., & Liang, S. (2009). Evaluation of ASTER and MODIS land surface temperature and emissivity products using long-term surface longwave radiation observations at SURFRAD sites. *Remote Sensing of Environment*, *113*(7), 1556–1565. https://doi.org/10.1016/j.rse.2009.03.009

Wang, Z., Schaaf, C. B., Chopping, M. J., Strahler, A. H., Wang, J., Roman, M. O., et al. (2012). Evaluation of Moderate-resolution Imaging Spectroradiometer (MODIS) snow albedo product (MCD43A) over tundra. *Remote Sensing of Environment*, *117*, 264–280. https://doi.org/10.1016/j.rse.2011.10.002

Wang, Z., Zeng, X., Barlage, M., Dickinson, R., Gao, F., & Schaaf, C. (2004). Using MODIS BRDF and albedo data to evaluate global model land surface albedo. *Journal of Hydrometeorology*, *5*(1), 3–14. https://doi.org/10.1175/1525-7541(2004)005<0003:umbaad>2.0.co;2

Wickham, J., Barnes, C. A., Nash, M. S., & Wade, T. G. (2015). Combining NLCD and MODIS to create a land cover-albedo database for the continental United States. *Remote Sensing of Environment*, *170*, 143–152. https://doi.org/10.1016/j.rse.2015.09.012

Wilson, K., Goldstein, A., Falge, E., Aubinet, M., Baldocchi, D., Berbigier, P., et al. (2002). Energy balance closure at FLUXNET sites. *Agricultural and Forest Meteorology*, *113*(1–4), 223–243. https://doi.org/10.1016/s0168-1923(02)00109-0

Wu, T., Lu, Y., Fang, Y., Xin, X., Li, L., Li, W., et al. (2019). The Beijing Climate Center Climate System Model (BCC-CSM): The main progress from CMIP5 to CMIP6. *Geoscientific Model Development*, *12*(4), 1573–1600. https://doi.org/10.5194/gmd-12-1573-2019

Wu, T., Zhang, F., Zhang, J., Jie, W., Zhang, Y., Wu, F., et al. (2020). Beijing Climate Center Earth System Model Version 1 (BCC-ESM1): Model description and evaluation of aerosol simulations. *Geoscientific Model Development*, *13*(3), 977–1005. https://doi.org/10.5194/gmd-13-977-2020

Xu, J., Zhang, X., Feng, C., Yang, S., Guan, S., Jia, K., et al. (2021). Evaluation of surface upward longwave radiation in the CMIP6 models with ground and satellite observations. *Remote Sensing*, *13*(21), 4464. https://doi.org/10.3390/rs13214464

Yao, Y., Liang, S., Li, X., Liu, S., Chen, J., Zhang, X., et al. (2016). Assessment and simulation of global terrestrial latent heat flux by synthesis of CMIP5 climate models and surface eddy covariance observations. *Agricultural and Forest Meteorology*, *223*, 151–167. https://doi.org/10.1016/j.agrformet.2016.03.016

Yukimoto, S., Kawai, H., Koshiro, T., Oshima, N., Yoshida, K., Urakawa, S., et al. (2019). The meteorological research institute Earth system model version 2.0, MRI-ESM2. 0: Description and basic evaluation of the physical component. *Journal of the Meteorological Society of Japan*. https://doi.org/10.2151/jmsj.2019-051

Zhang, X., Liang, S., Wang, K., Li, L., & Gui, S. (2010). Analysis of global land surface shortwave broadband albedo from multiple data sources. *IEEE Journal of Selected Topics in Applied Earth Observations and Remote Sensing*, *3*(3), 296–305. https://doi.org/10.1109/jstars.2010.2049342

Zhang, X., Liang, S., Wild, M., & Jiang, B. (2015). Analysis of surface incident shortwave radiation from four satellite products. *Remote Sensing of Environment*, *165*, 186–202. https://doi.org/10.1016/j.rse.2015.05.015

Zhou, Y., Wang, D., Liang, S., Yu, Y., & He, T. (2016). Assessment of the Suomi NPP VIIRS land surface albedo data using station measurements and high-resolution albedo maps. *Remote Sensing*, *8*(2), 137. https://doi.org/10.3390/rs8020137

Zhu, X., Lee, S.-Y., Wen, X., Wei, Z., Ji, Z., Zheng, Z., & Dong, W. (2021). Historical evolution and future trend of Northern Hemisphere snow cover in CMIP5 and CMIP6 models. *Environmental Research Letters*. https://doi.org/10.1088/1748-9326/ac0662